Representation of distinct reward variables for self and other in primate lateral hypothalamus

Atsushi Noritake[a,b,c], Taihei Ninomiya[a,b], and Masaki Isoda[a,b,c,1]

[a]Division of Behavioral Development, Department of System Neuroscience, National Institute for Physiological Sciences, National Institutes of Natural Sciences, Okazaki, Aichi 444-8585, Japan; [b]Department of Physiological Sciences, School of Life Science, The Graduate University for Advanced Studies, Hayama, Kanagawa 240-0193, Japan; and [c]Department of Physiology, Kansai Medical University School of Medicine, Hirakata, Osaka 573-1010, Japan

Edited by Matthew F. S. Rushworth, Oxford University, Oxford, United Kingdom, and accepted by Editorial Board Member Leslie G. Ungerleider January 27, 2020 (received for review October 2, 2019)

The lateral hypothalamus (LH) has long been implicated in maintaining behavioral homeostasis essential for the survival of an individual. However, recent evidence suggests its more widespread roles in behavioral coordination, extending to the social domain. The neuronal and circuit mechanisms behind the LH processing of social information are unknown. Here, we show that the LH represents distinct reward variables for "self" and "other" and is causally involved in shaping socially motivated behavior. During a Pavlovian conditioning procedure incorporating ubiquitous social experiences where rewards to others affect one's motivation, LH cells encoded the subjective value of self-rewards, as well as the likelihood of self- or other-rewards. The other-reward coding was not a general consequence of other's existence, but a specific effect of other's reward availability. Coherent activity with and top-down information flow from the medial prefrontal cortex, a hub of social brain networks, contributed to signal encoding in the LH. Furthermore, deactivation of LH cells eliminated the motivational impact of other-rewards. These results indicate that the LH constitutes a subcortical node in social brain networks and shapes one's motivation by integrating cortically derived, agent-specific reward information.

lateral hypothalamus | self | other | reward | macaque

The hypothalamus is an evolutionarily conserved region in the tetrapod brain (1). Among its several anatomical divisions, the lateral hypothalamus (LH) coordinates diverse behavioral roles essential for the survival of an individual (2–4), such as arousal and sleep–wake transitions (5, 6), reward-seeking (7), stress and anxiety (8, 9), and learning and memory (10, 11), through anatomical connections among the forebrain–brainstem axis (4, 12–14). However, more recent work from behavioral and imaging studies suggests that the role for the LH in behavioral coordination may extend to include social aspects. Specifically, photoactivation of LH cells projecting to the dopamine-rich ventral tegmental area facilitates social interactions in rodents (15). Moreover, in functional neuroimaging studies, the volume of the LH and adjacent structures is increased with increasing social hierarchy in macaques (16) and decreased in people with autism spectrum disorder (17), which is characterized by deficient social interactions. These findings across different mammalian species raise the possibility that the LH plays a key role in social cognition and interactions. However, research into the social domain of LH functions is still in its infancy. Accordingly, what social information is specifically processed by LH cells and what neural circuits underlie such social information processing remain unknown.

To address these issues, we introduced a Pavlovian conditioning procedure extended to a self-and-other context using pairs of monkeys (18) and recorded neural activity from one monkey in each pair. In this procedure, we incorporated aspects of social comparison (19) and resource limitation by manipulating reward probabilities for self and other. We show that LH cells first encode a subjective value of own rewards by taking account of other-reward information and then encode the likelihood of rewards separately for the self and other. We also demonstrate that coherent activity with and top-down information flow from the medial prefrontal cortex (MPFC), a hub of social brain networks (20), contributes to signal encoding in the LH. Combined with intervention experiments, we propose that the LH is an integral component of social brain networks and shapes motivated behavior in social contexts.

Results

Each trial started when a visual conditioned stimulus was presented at the center of a monitor, which was positioned equidistantly from each monkey (Fig. 1 *A*, *Top*). Two blocks of trials were alternately run, in each of which different visual stimuli ($n = 3$) predicted liquid reward delivery to the self (recorded monkey, designated as M1) and its partner (nonrecorded monkey, designated as M2) with different probabilities. Specifically, in the M1-variable block (Fig. 1 *A*, *Bottom*), the probability of the M1-reward varied depending on which of three stimuli was presented ($P = 0.25$, $P = 0.5$, and $P = 0.75$), but the probability of the M2-reward was invariable ($P = 0.2$). In the M2-variable block, the probability of the M2-reward varied depending on which of three other stimuli was presented ($P = 0.25$, $P = 0.5$, and $P = 0.75$), but the probability of the M1-reward was invariable ($P = 0.2$). After 1 s of stimulus presentation ("stimulus period"), the reward outcome, either the delivery or omission of a reward, was revealed first to M2 and 1 s later to M1 (Fig. 1 *A*,

Significance

Motivation is affected by rewards to both oneself and others. Which brain regions separately monitor self-rewards and other-rewards? It has been thought that higher-order, neocortical regions, such as the medial prefrontal cortex, monitor behavioral information in agent-selective manners. Here, we show that a subcortical region called the lateral hypothalamus (LH), an evolutionarily old structure in the vertebrate brain, also contains agent-specific reward information and further integrates it into a subjective reward value. This other-reward–dependent value signal is causally used for adaptive behavior, because deactivation of LH cells totally eliminates the motivational impact of other-rewards. Our findings indicate that the LH is an integral component of social brain networks and shapes socially motivated behavior via functional coordination with neocortical regions.

Author contributions: A.N. and M.I. designed research; A.N., T.N., and M.I. performed research; A.N. and T.N. analyzed data; and A.N., T.N., and M.I. wrote the paper.

The authors declare no competing interest.

This article is a PNAS Direct Submission. M.F.S.R. is a guest editor invited by the Editorial Board.

[1]To whom correspondence may be addressed. Email: isodam@nips.ac.jp.

This article contains supporting information online at https://www.pnas.org/lookup/suppl/doi:10.1073/pnas.1917156117/-/DCSupplemental.

First published February 24, 2020.

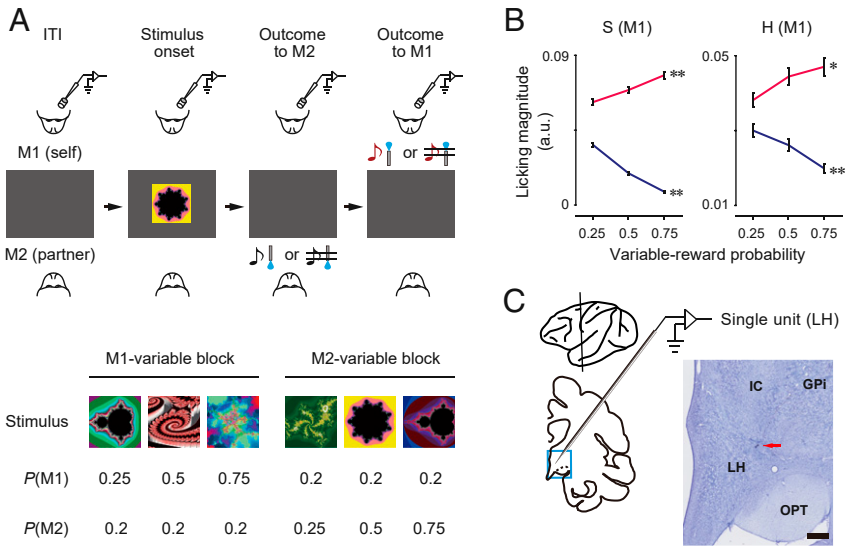

Fig. 1. Experimental paradigm and behavioral evidence for subjective value modulation. (*A*, *Top*) Social Pavlovian conditioning. Black and red musical notes depict low- and high-pitch tones, respectively. (*A*, *Bottom*) Reward probability matrix. *P*(M1), probability of M1-reward. *P*(M2), probability of M2-reward. (*B*) Subjective value modulation. Mean ± SEM. Variable-reward probability indicates the M1-reward probability in the M1-variable block (red) and the M2-reward probability in the M2-variable block (blue). $^{**}P < 0.01$; $^{*}P < 0.05$. (*C*) Recording sites. Nissl-stained section for the area indicated by the blue rectangle. (Scale bar, 1 mm.) Red arrow, electrolytic microlesion made at the entry point into the LH. IC, internal capsule; OPT, optic tract; GPi, internal globus pallidus.

Top). A reward to M2 and M1 was accompanied by a low-pitch tone and a high-pitch tone, respectively (Fig. 1 *A*, *Top*). The three stimuli in each block were presented in a pseudorandom order with equal frequency (*SI Appendix*, Fig. S1*B*).

We incorporated aspects of resource limitation into the procedure, such that M1 could be rewarded, albeit not always, only when M2 was not rewarded (*SI Appendix*, Fig. S1*A*). Under this constraint, the probability of the M1-reward changed conditionally upon the outcome of M2 (*SI Appendix*, Fig. S1 *C* and *D*). However, the number of M1-rewarded trials was eventually the same between all three stimuli in the M2-variable block (eight trials per stimulus; *SI Appendix*, Fig. S1*B*). Thus, the probability of the M1-reward during the stimulus period was exactly the same in the M2-variable block ($P = 0.2$), regardless of which stimulus was presented, as opposed to the M1-variable block.

We used four macaque monkeys (S, H, B, and D) in two pairs, S–B and H–D, in which monkeys S and H served as M1. Both of the M1 monkeys showed anticipatory licking behavior during the stimulus period, the magnitude of which increased as the probability of the M1-reward increased (monkey S, $n = 690$ blocks, $P = 4.6 \times 10^{-9}$, Spearman rank correlation test; monkey H, $n = 322$, $P = 2.4 \times 10^{-2}$; Fig. 1*B*, red). Notably, the magnitude of anticipatory licking was decreased as the probability of the M2-reward increased (monkey S, $n = 690$ blocks, $P = 3.5 \times 10^{-142}$; monkey H, $n = 322$, $P = 1.7 \times 10^{-4}$; Fig. 1*B*, blue), although M1 ended in reward gains objectively with equal frequency. This finding indicates that the value of one's own reward is subjectively lowered by a higher incidence of rewards to conspecifics. Note that, in our behavioral procedure, the order of outcome revelation and the context of resource limitation were both critical factors for the emergence of subjective value modulation, as reported previously (18).

The activity of single LH cells ($n = 379$) was recorded in the two M1 monkeys (Fig. 1*C*) in accordance with a physiological protocol described previously (21). Our analysis was focused on the stimulus period, in which subjective value modulation was observed. The stimulus period was divided further into early (151 to 450 ms from stimulus onset) and late (701 to 1,000 ms) epochs.

Consistent with a previous study (21), approximately one-third of the recorded cells ($n = 139$) exhibited a phasic response during the early epoch that was either positively or negatively correlated with the M1-reward probability ($P < 0.01$, Spearman rank correlation test; *SI Appendix*, Fig. S2*A*, red and yellow dots). Interestingly, 29 of these cells additionally exhibited a phasic response that was now correlated with the M2-reward probability in an opposite manner ($P < 0.01$, Spearman rank correlation test; *SI Appendix*, Fig. S2*A*, yellow dots), as exemplified by the cells shown in Fig. 2 *B* and *C*. This response profile showed a resemblance to the anticipatory licking behavior (Fig. 1*B*), suggesting a close relationship between the LH cell response and the behavioral manifestation of subjective value. Although the remaining cells ($n = 110$) were not significantly modulated by the M2-reward probability on a cell-by-cell basis, a gross inspection of the early-epoch activity of all sampled cells (Fig. 2*A*, red arrowheads) provided an impression that the more positive a correlation was between activity and M1-reward probability, the more negative it was between activity and M2-reward probability, and vice versa. To formally test this potential inverse relationship at the population level, we took independent measures of each cell's sensitivity (regression slope) to the M1-reward and M2-reward probabilities. This analysis revealed a significant negative correlation between the two slopes across all of the recorded cells (Fig. 2*G*; $\rho = -0.43$, $P = 4.2 \times 10^{-18}$, Spearman rank correlation test). These findings suggest that directly after stimulus presentation, LH cells inherently encoded a subjective, not objective, value at the population level by taking the partner–reward information into account.

This inverse relationship was not observed in the late epoch (Fig. 2*D*, red arrowheads). The strength of the negative correlation reached a maximum at the midearly epoch and was quickly rendered nonsignificant (Fig. 2*H*). Instead, response categorization on a cell-by-cell basis revealed the emergence of two distinct types of social reward variable: the likelihood of a reward being delivered to the self and the likelihood of a reward being delivered to the partner. The self-reward signal was encoded by a subset of cells (self-type cells, $n = 52$; $n = 33$ from monkey S, $n = 19$ from monkey H; Fig. 2*I*, red dots) that exhibited monotonically increasing (positive type; Fig. 2*E* and *SI Appendix*, Fig. S3*A*)

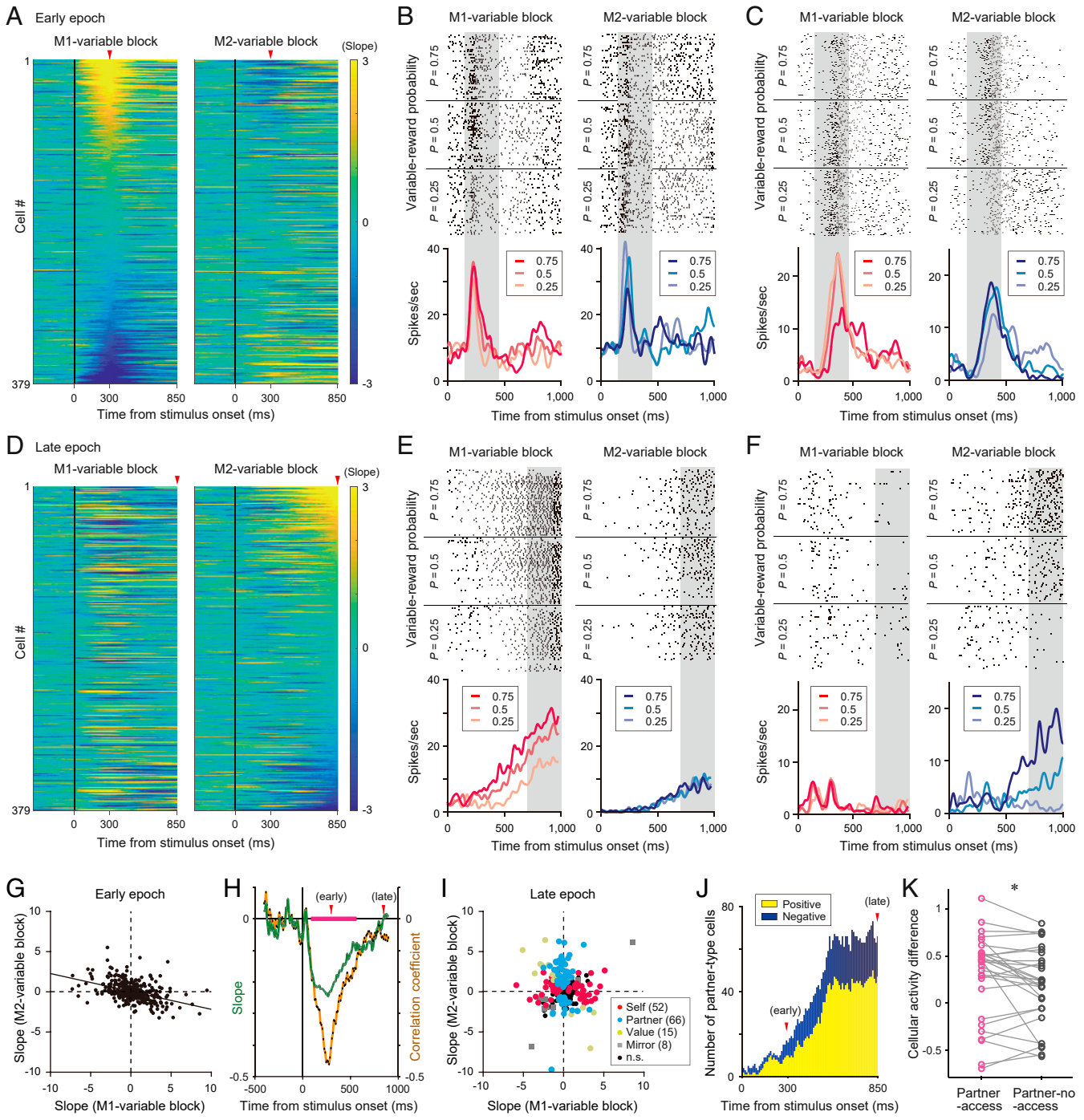

Fig. 2. Time-dependent reward variables encoded by LH cells. (*A*) Moving-window plots of regression slopes. Cells are sorted according to the regression slopes in the early epoch in the M1-variable block. Window width, 300 ms; moving step, 10 ms. Values on the time axis indicate the center times of each moving window (e.g., red arrowheads at 300 ms indicate data between 151 and 450 ms corresponding to the early epoch). (*B*) Raster plots and spike density functions of an LH cell showing a positive correlation with the M1-reward probability and a negative correlation with the M2-reward probability in the early epoch (indicated by grayed areas). Note that this subjective value-type cell in the early epoch is classified as the self type in the late epoch. *Insets* indicate the variable-reward probability. (*C*) Activity of an LH cell showing a negative correlation with the M1-reward probability and a positive correlation with the M2-reward probability in the early epoch (grayed areas). (*D*) Moving-window plots of regression slopes. Same dataset as in *A*, but the cells are sorted according to the slopes in the late epoch (red arrowheads) in the M2-variable block. (*E*) A self-type LH cell defined in the late epoch (grayed areas). (*F*) A partner-type LH cell defined in the late epoch (grayed areas). (*G*) Scatter plot of the regression slope in the early epoch. One point per cell. (*H*) Moving-window plot of the regression slope and correlation coefficient. Window width, 200 ms; moving step, 10 ms. Pink bar indicates the points at which Spearman's correlation coefficient was significant ($P < 0.05$). (*I*) Scatter plot of the regression slope in the late epoch. See *Materials and Methods* for the definition of each cell type. Values in parentheses indicate numbers of cells. (*J*) Moving-window plot of the number of partner-type cells. Window width, 300 ms; moving step, 10 ms. (*K*) Cellular activity difference for the partner-type cells measured in the late epoch. *$P = 0.035$, paired *t* test. One point per cell. This index represents a difference in responses to the most [P(M2) = 0.75 for the positive type and P(M2) = 0.25 for the negative type] and least [P(M2) = 0.25 for the positive type and P(M2) = 0.75 for the negative type] preferred stimuli for each cell in the M2-variable block.

or decreasing (negative type; *SI Appendix*, Fig. S3*B*) activity as the M1-reward probability increased; here, the activity was nondifferential for the M2-reward probability. The partner-reward signal was encoded by another subset of cells (partner-type cells, $n = 66$; $n = 40$ from monkey S, $n = 26$ from monkey H; Fig. 2*I*, blue dots) that exhibited monotonically increasing (positive type; Fig. 2*F* and *SI Appendix*, Fig. S3*C*) or decreasing (negative type; *SI Appendix*, Fig. S3*D*) activity as the M2-reward probability increased; here, the activity was nondifferential for the M1-reward probability. The number of partner-type cells increased rapidly after the midearly epoch and reached a plateau before and during the late epoch (Fig. 2*J*). These findings demonstrated time-dependent changes of social reward coding in the LH, i.e., subjective value coding in the early epoch and agent-specific reward coding in the late epoch.

The time-dependent LH signal raises a critical question of whether the two types of cells, i.e., those encoding a subjective value and those encoding agent-specific reward information, are two separate populations, or whether the same cells change their coding scheme over time. A close inspection of the cell shown in Fig. 2*B* revealed a transition from the subjective-value coding in the early epoch to the self-reward coding in the late epoch (positive self-type). We found that, among the subjective-value–type cells categorically classified in the early epoch, almost one-half ($n = 14/29$) were judged to encode agent-specific reward information in the late epoch (self type, $n = 4$; partner type, $n = 10$), consistent with the change in coding scheme by the same cells. By contrast, there were also cells that encoded only the subjective-value information in the early epoch (11/29) or only the agent-specific reward information in the late epoch ($n = 48/118$; self type, $n = 15/52$; partner type, $n = 33/66$). This analysis, performed on a cell-by-cell basis, suggests that the transition of information during the stimulus period was mediated by both "transition" cells and "nontransition" cells. Interestingly, when a scatter plot was constructed in the same format as in Fig. 2*G* but now using only the cells with agent-specific reward coding defined in the late epoch, we still identified a significant negative correlation in the early epoch for both the self-type (*SI Appendix*, Fig. S2 *B*, *Top*; $n = 52$, $\rho = -0.49$, $P = 2.4 \times 10^{-4}$; Spearman rank correlation test) and the partner-type cells (*SI Appendix*, Fig. S2 *B*, *Bottom*; $n = 66$, $\rho = -0.58$, $P = 4.9 \times 10^{-7}$; Spearman rank correlation test). These findings again suggest that the population of LH cells inherently encode the subjective value in the early epoch and change their coding scheme to the agent-specific reward in the late epoch.

We considered the possibility that the emergence of agent-specific reward coding in the late epoch might be associated with an increase over time in looking at M1's reward spout in the M1-variable block in anticipation of the self-reward, or an increase over time in looking at M2 in the M2-variable block in anticipation of the partner reward. Such changes in gaze behavior could explain, at least in part, why the neuronal reference frame shifts from common value coding to agent-specific coding. We found, however, that both M1 monkeys looked at the stimulus on the display for a longer period of time during the late epoch than during the early epoch (*SI Appendix*, Fig. S4 *B* and *E*, *Middle*; monkey S, $P = 3.5 \times 10^{-299}$ for M1-variable block, $P = 3.0 \times 10^{-288}$ for M2-variable block, $n = 688$ blocks; monkey H, $P = 1.4 \times 10^{-56}$ for M1-variable block, $P = 6.8 \times 10^{-105}$ for M2-variable block, $n = 320$ blocks; paired t test). More importantly, the duration of gaze around M1's spout in the M1-variable block was significantly decreased over time (*SI Appendix*, Fig. S4 *C* and *F*, *Middle*; monkey S, $P = 2.1 \times 10^{-149}$, $n = 688$ blocks; monkey H, $P = 4.8 \times 10^{-41}$, $n = 320$ blocks; paired t test). Likewise, the duration of gaze at M2 in the M2-variable block was significantly decreased (*SI Appendix*, Fig. S4 *A*, *Middle*; monkey S, $P = 1.3 \times 10^{-75}$, $n = 688$ blocks; paired t test) or did not change over time (*SI Appendix*, Fig. S4 *D*, *Middle*; monkey H, $P = 0.35$, $n = 320$ blocks; paired t test). In fact, both M1 monkeys rarely observed the partner or the self-spout region in the late epoch. These findings suggest that the shift of the neuronal reference frame cannot be accounted for by gaze behavior. It should be noted, however, that the M1 monkeys monitored the M2-reward outcome once it was revealed. Specifically, M1 looked at M2 significantly longer when M2 was rewarded than when M2 was not rewarded (*SI Appendix*, Fig. S4 *A* and *D*, *Right*; monkey S, $P = 5.7 \times 10^{-5}$ for M1-variable block, $P = 8.3 \times 10^{-64}$ for M2-variable block, $n = 688$ blocks; monkey H, $P = 5.9 \times 10^{-6}$ for M1-variable block, $P = 1.3 \times 10^{-7}$ for M2-variable block, $n = 320$ blocks; paired t test). By contrast, M1 looked at M1's spout region significantly longer when M2 was not rewarded than when M2 was rewarded (*SI Appendix*, Fig. S4 *C* and *F*, *Right*; monkey S, $P = 9.8 \times 10^{-238}$ for M1-variable block, $P = 4.6 \times 10^{-251}$ for M2-variable block, $n = 688$ blocks; monkey H, $P = 1.2 \times 10^{-20}$ for M1-variable block, $P = 6.5 \times 10^{-63}$ for M2-variable block, $n = 320$ blocks; paired t test).

We previously showed that the MPFC, a hub of social brain networks (20), contains both self-type cells and partner-type cells in the reward domain (18). Therefore, it is tempting to hypothesize that the LH is functionally coordinated with the MPFC. Supporting this view, the two regions form a functional network during cue–reward associations in a Pavlovian conditioning paradigm (10), and the LH receives afferent inputs from the MPFC (12, 14). To test this possibility more directly, local field potentials (LFPs) were recorded simultaneously in the MPFC and LH using 16-channel electrodes (Fig. 3*A*). Here, bipolar derivations of LFPs were obtained by successively rereferencing each channel (excluding the most superficial) to the next channel in the superficial direction to remove spurious estimates of coordinated activity (22), such as those due to a common reference. We found that the latency distribution of stimulus-locked LFPs differed significantly between the two regions: The MPFC response occurred substantially earlier than the LH response (Fig. 3*B*; MPFC median = 89 ms, $n = 362$ contacts; LH median = 188 ms, $n = 227$; $P = 7.4 \times 10^{-41}$, Kolmogorov–Smirnov test). Moreover, the coherence of LFPs between both regions prominently increased after stimulus onset, particularly at frequencies below ~20 Hz, in both the M1-variable and M2-variable blocks (Fig. 3*C*). Furthermore, Granger causality during both task epochs was significantly greater in the MPFC-to-LH direction than in the LH-to-MPFC direction in virtually all frequency bands (Fig. 3*D*). These findings demonstrated the importance of MPFC–LH coordination in social reward processing and suggested that top-down information flow from the MPFC contributed to signal encoding in the LH.

What might be the impact of partner's reward contexts on LH activity? We previously reported that subjective value modulation, as indexed by the licking movement, was absent in the M2-variable block when the partner monkey was replaced with a water-collecting bottle (18). We also reported that the subjective value modulation, as indexed by the licking and choice behaviors, was significantly attenuated or absent in the M2-variable block when the partner monkey was present in front of M1 but was deprived of access to a reward (18). In this partner–no-access condition, the reward spout was removed from M2's mouth, such that a reward was no longer available to M2, and thus M2-reward was no longer relevant to M1, even if the low-pitch tone was presented (*SI Appendix*, Fig. S2 *C*, *Left*). This finding ruled out the possibility that the subjective value modulation was caused by a potential negative association formed by the low-pitch tone indicating reward delivery to M2. Here we studied, then, how partner's reward availability might affect activity of partner-type LH cells. We found that the cellular activity difference, defined as a difference in responses to the most and least preferred stimuli for each cell, were significantly decreased in the late epoch when switched from the partner–access condition (i.e., original social condition) to the partner–no-access condition ($n = 29$, $P = 0.035$, paired t test; Fig. 2*K*). Moreover, activity during

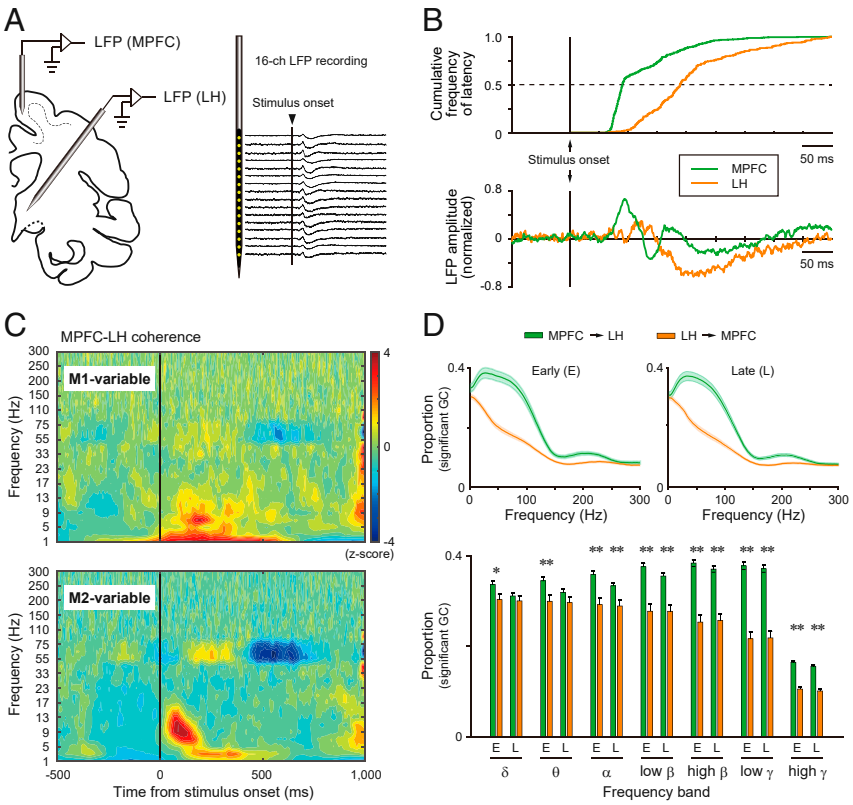

Fig. 3. Dual-site simultaneous LFP recording. (*A*) Experimental setup. (*B*) Comparison of stimulus-locked LFP. (*Top*) Cumulative frequency plot of response latency. (*Bottom*) Ensemble-averaged normalized LFP. (*C*) Coherence between MPFC-LFP and LH-LFP. $n = 34$ sessions. (*D*) Granger causality (GC) analysis. Mean ± SEM. (*Top*) Proportion of LFP pairs with significant GC in specified directions. (*Bottom*) Comparison of significant GC between the top-down direction (green) and bottom-up direction (orange) for each frequency band. Data in both blocks were combined. δ, 1 to 3 Hz; θ, 4 to 7 Hz; α, 8 to 12 Hz; low β, 13 to 20 Hz; high β, 21 to 30 Hz; low γ, 31 to 49 Hz; high γ, 50 to 300 Hz. $*P < 0.05$, $**P < 0.001$, Welch's *t* test. $n = 34$ sessions.

the early epoch was not significantly affected by the M2-reward probability ($P = 0.60$, Spearman rank correlation test; *SI Appendix*, Fig. S2 *C*, *Right*). Thus, the observed reduction or lack of cellular activity modulation could be associated with the decrease in licking modulation when the partner-reward was no longer relevant. These findings suggest that the partner's reward availability is a critical factor to determine the response magnitude of LH cells.

If the social reward signals in the LH are crucial for the control of motivated behavior, then deactivation of this area is likely to attenuate subjective value modulation. We confirmed that this was the case by reversible inactivation of LH cells with the local application of muscimol, a γ-aminobutyric acid agonist (Fig. 4*A*). The injection of muscimol into the unilateral LH caused a significant decrease in sensitivity to both M1-reward and M2-reward probabilities, as indicated by significant interactions

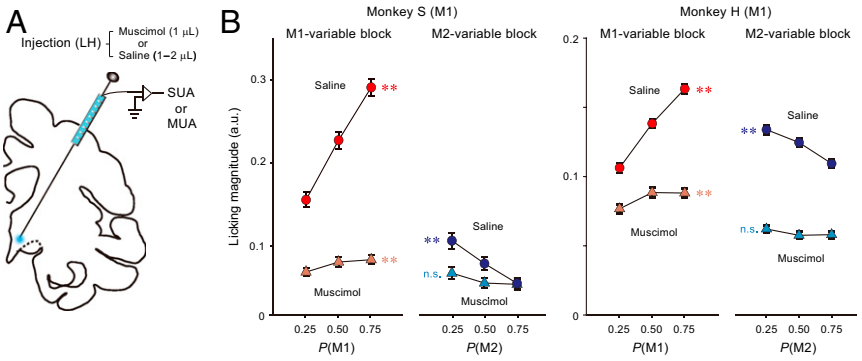

Fig. 4. Effects of muscimol injection into the LH. (*A*) Experimental setup. MUA, multiunit activity; SUA, single-unit activity. (*B*) Subjective value modulation after muscimol (solid triangles) or saline (solid circles) injection. Mean ± SEM. $**P < 0.001$, Spearman rank correlation test. Interactions between injection substance and reward probability by ANOVA; monkey S, $P = 4.8 \times 10^{-14}$ for the M1-variable block, $P = 0.036$ for the M2-variable block; monkey H, $P = 8.9 \times 10^{-10}$ for the M1-variable block, $P = 0.0010$ for the M2-variable block. $n = 2{,}515$ trials (S, M1-variable, saline), 3,240 (S, M1-variable, muscimol), 2,327 (S, M2-variable, saline), 2,880 (S, M2-variable, muscimol); $n = 1{,}981$ trials (H, M1-variable, saline), 2,018 (H, M1-variable, muscimol), 2,074 (H, M2-variable, saline), and 2,008 (H, M2-variable, muscimol).

between injection substance and reward probability (all $P < 0.05$, two-way analysis of variance [ANOVA]; Fig. 4*B*), compared to control conditions in which saline was injected at the same location. After muscimol injections, positive correlations were still significant between licking magnitude and M1-reward probability (monkey S, $\rho = 0.051$, $P = 0.0036$; monkey H, $\rho = 0.062$, $P = 0.0049$; Spearman rank correlation test). Notably, negative correlations were no longer significant between licking magnitude and M2-reward probability (monkey S, $\rho = -0.033$, $P = 0.070$; monkey H, $\rho = -0.029$, $P = 0.19$; Spearman rank correlation test).

Discussion

Using a Pavlovian conditioning procedure extended to a self-and-other context, we have demonstrated that the LH is causally involved in shaping socially motivated behavior by taking account of other-reward information. LH cells implement this function by processing distinct social reward variables in a time-dependent manner. Dual-site LFP recordings suggest that phase synchronization with, and top-down information flow from, the MPFC underlie signal encoding in the LH. The interareal coherence predominates in the beta and lower bands, which is overall consistent with interareal influences in the visual system (23). Furthermore, encoding of other-reward information is not a general effect of other's existence per se, but a specific effect of other's access to rewards. These findings indicate that the LH plays an important role in adaptive social behavior.

The LH has been considered a heterogenous assembly of cell populations, most typically defined by neurochemical markers (4). Therefore, it is noteworthy that the whole population of LH cells became transiently, but uniformly, tuned to a reward value in the subjective scale. This value coding during the early epoch apparently resembles that in the dopaminergic midbrain nuclei (18). However, unlike dopaminergic cells where value signals are unidirectional (i.e., existence of only positive type), value signals in LH cells are bidirectional (i.e., existence of both positive and negative types). This response property suggests that LH cells encode a subjective reward value in two opposing axes, i.e., how "undesirable" (negative type) as well as how "desirable" (positive type) the expected outcome would be in a given social environment. The existence of such undesirability coding would allow organisms to make a critical social decision more directly and quickly, especially when relevant options should be avoided. The avoidance of response options that are of low social value may be mediated by LH-to-habenula projections (24).

The neural information in the LH changed drastically during the late epoch. Specifically, most LH cells were now categorically classified into two distinct populations, i.e., one selectively encoding the likelihood of the self-reward and the other selectively encoding the likelihood of the partner-reward. A rise of activity in the late epoch suggests that these cells encode reward anticipation separately for the self and other. This agent-specific reward coding is strikingly similar to that in the MPFC (18). The existence of LH cells conveying other-specific information is surprising, given that this subcortical region is evolutionarily conserved (1) and has long been implicated in behavioral control fundamental for the survival of an individual. The agent-specific reward coding is virtually absent in the dopaminergic midbrain nuclei under the same behavioral condition (18), suggesting that the LH is more like a cortical area with respect to the distinction between aspects of the self and others. However, such agent-specific coding in subcortical regions is not confined to the LH; a recent study showed that primate amygdala cells during observational learning encode own choices and partner's predicted choices in an agent-specific manner (25). Interestingly, amygdala cells often encoded the value of the partner-reward in the same way as they encoded own reward value (25, 26). By contrast, such mirroring of reward-value encoding was rarely observed in the present study (mirror-type cells, $n = 1$ in the early epoch, $n = 8$ in the late epoch). This difference could be explained by a difference in experimental design. In our study, the exclusive reward schedule mimicking resource limitation was introduced, which might have promoted the anticorrelated value coding between the self and other. By contrast, the amygdala studies lacked such a behavioral element as resource limitation and instead involved prosocial choices (26) and observational learning (25).

One may argue that the observation of M2's anticipatory licking could affect M1's anticipatory licking in the M2-variable block, which in some way influences the subjective value modulation. Indeed, we previously showed using the same monkey pairs that M2's licking movement was increased as the M2-reward probability was increased (18). However, we also observed that the M2's licking was not systematically affected by the M1's licking in the M1-variable block (18). This finding implies that others' licking movement does not automatically facilitate similar movement, or inhibit ongoing licking movement, in the observer's face, unlike other forms of motor or emotional mirroring, such as rapid facial mimicry (27). Moreover, as we observed in the present study (*SI Appendix*, Fig. S4), M1 monkeys rarely looked at M2 during the stimulus period. We therefore conjecture that the M2's anticipatory licking had a negligible impact, if any, on M1's value modulation. Instead, we hypothesize that the subjective value modulation was mostly formed by learned associations between the visual stimuli and partner's reward outcomes. In support of this view, M1 monitored M2 significantly longer when M2 was rewarded than when M2 was not rewarded (*SI Appendix*, Fig. S4). It should be also noted that, as mentioned above, the subjective value modulation was absent in the M2-variable block when M2 was replaced with a water-collecting bottle (18), which ruled out the possibility that the value modulation was caused by a potential negative association with the low-pitch tone per se.

The response latency difference and the directional bias of information flow suggest that the agent-specific reward signals in the LH originate from the MPFC. It is also possible, however, that the signal transmission is not entirely unilateral: The LH signal may be sent back to the MPFC via bottom-up projections (13, 28), acting as a type of reverberating circuits as previously reported between top-down and bottom-up projections (29). This mechanism may contribute to the persistent coding of agent-specific information along the cortico-subcortical pathway.

Deactivation of LH cells by muscimol injections caused a decrease in sensitivity to both the self-reward probability and partner-reward probability. In particular, the effects of the partner-reward probability on the licking movement disappeared after muscimol injections, while those of the self-reward probability remained, albeit weakly. However, this finding may not directly indicate that the LH plays a more important role in the other-reward processing compared to the self-reward processing. This is because the effect size of the partner-reward probability was generally smaller than that of the self-reward probability without muscimol injections at both the behavioral (Fig. 4*B*) and neuronal levels (Fig. 2*G*). Nonetheless, our findings clearly show that the LH is involved in socially motivated behavior by taking other-reward information into account.

In summary, the present findings lead to a proposal that the LH is an integral component of social brain networks and shapes socially motivated behavior via functional coordination with the MPFC. The role for the LH in behavioral coordination is more widespread than currently understood and now extends to include the social domain. Further investigation is required to clarify the in-depth neural mechanisms by which information carried by LH cells swiftly changes over hundreds of milliseconds and to determine how the LH communicates with other subcortical regions, such as the dopaminergic midbrain nuclei, during social interactions. These questions are testable using our experimental paradigm.

Materials and Methods

Animals. Four male macaques (*Macaca fuscata*, monkeys S [age 7], H [age 4], and D [age 5]; *Macaca fascicularis*, monkey B [age 10]) were used as subjects of this study. All animal care and experimentation protocols were approved by the Institutional Animal Care and Use Committee of National Institutes of Natural Sciences and Kansai Medical University and were carried out in accordance with the guidelines described in the National Institutes of Health *Guide for the Care and Use of Laboratory Animals* (30), as reported previously (18).

Behavioral Procedures.

Social Pavlovian conditioning procedure (partner–access condition). Each pair of two monkeys were placed in a sound-shielded room and were conditioned with visual stimuli using a Pavlovian procedure. Monkey S was paired with monkey B, and monkey H was paired with monkey D. The monkeys in each pair were not cage mates; therefore, their fixed dominance relationship was not determined. In the two pairs, we recorded from monkeys S and H. The recorded monkeys are herein referred to as M1 or self, and the nonrecorded monkeys are referred to as M2 or partner.

As described in detail elsewhere (18), the two monkeys in each pair sat in individual primate chairs and faced each other across a horizontally placed liquid crystal display monitor, which was positioned at the center of the two monkeys (Fig. 1 *A*, *Top*). The distance between the two monkeys was 110 cm at eye level. Each trial started when a visual fractal stimulus (188 mm × 202 mm) was presented at the center of the monitor; both animals were able to see the stimulus directly. After 1 s, the stimulus went off and the reward outcome, either delivery or omission of a reward (water), was revealed first to M2 and 1 s later to M1. A low-pitch tone (125 Hz) and high-pitch tone (1 kHz) were presented along with the reward delivery to M2 and M1, respectively. The two different tones were used to facilitate the association between each tone and each agent's reward and to better differentiate between the self and partner's reward delivery. During neural data collection, the monkeys were not required to fixate any stimulus.

The conditioning procedure was performed in two trial blocks that differed in reward contexts: the "M1-variable block" and the "M2-variable block," each consisting of 120 trials (Fig. 1 *A*, *Bottom*, and *SI Appendix*, Fig. S1*B*). In the M1-variable block, we used three different visual stimuli. Each stimulus was associated with M1-reward at a different probability ($P = 0.25$, $P = 0.5$, or $P = 0.75$), while all of the three stimuli were associated with M2-reward at the same probability ($P = 0.2$). In the M2-variable block, we used another three stimuli. Here, each stimulus was associated with M2-reward at a different probability ($P = 0.25$, $P = 0.5$, or $P = 0.75$), while all of the three stimuli were associated with M1-reward at the same probability ($P = 0.2$). The two trial blocks were alternately run during data recording. For each monkey, the total amount of reward earned was the same between the two blocks.

We incorporated into the procedure a behavioral constraint mimicking resource limitation in the natural world: that is, both animals were never rewarded on the same single trial. This indicates that M1 had a chance to receive a reward only when M2 had not been rewarded. Thus, the outcome at the end of each trial was one of the following: M2 rewarded, M1 rewarded, or neither rewarded (*SI Appendix*, Fig. S1*A*). Because of this behavioral constraint, M1-reward probability changed in both M1-variable and M2-variable blocks after the outcome was revealed to M2 (*SI Appendix*, Fig. S1 *C* and *D*). However, the focus of analysis was on a period during which a stimulus was presented ("stimulus period") before any outcome was revealed to M2. During this stimulus period, the probability of M1-reward was invariable across different stimuli in the M2-variable block (*SI Appendix*, Fig. S1*D*). Note that the number of M1-rewarded trials was indeed the same between the three stimuli in the M2-variable block (i.e., eight trials per stimulus; *SI Appendix*, Fig. S1*B*).

Partner–no-access condition. This condition was introduced to study how behavioral and neuronal modulations determined by the prospect of M2-rewards might differ depending on the M2's reward availability. For this purpose, we analyzed M1's anticipatory licking and LH activity during the stimulus period in the M2-variable block. In this condition, M2 was present, but its reward spout was removed. Thus, M2 was unable to receive a reward even if the low-pitched tone was produced. Instead, rewards were collected in a bottle placed beside the primate chair.

Surgical Procedures. The monkeys were anesthetized with intramuscular injections of ketamine HCl (10 mg/kg) and xylazine (1 to 2 mg/kg), and then maintained at a general anesthetic state with isoflurane (1 to 2%). After the skull was exposed, acrylic screws were installed to fasten dental acrylic head implant to the skull under aseptic surgical conditions, as described previously (18). A nonmetal head holder and recording chambers were positioned stereotaxically and secured with dental acrylic. Craniotomy was performed after the monkeys had been trained on the behavioral procedures described above. Antibiotics and analgesics were administered after surgery.

Behavioral Recording Procedures. Licking movements were sampled at 1 kHz, filtered (100 to 200 kHz), and amplified using a vibration sensor attached to the reward spout (AE-9922; NF Corporation). Eye position was sampled using an infrared video tracking system at a time resolution of 500 Hz and a spatial resolution of 0.1° (EyeLink II, SR Research; iRecHS2, Human Informatics Research Institute, National Institute of Advanced Industrial Science and Technology). Water rewards were delivered through a spout, which was under control of a solenoid valve. The solenoid valve was placed outside the sound-shielded room. The monkeys' overt movements were monitored constantly using a video-capturing system. Stimulus presentation, behavioral data collection, and reward delivery were controlled by a real-time experimentation data acquisition system (Tempo; Reflective Computing) or a personal computer running the MonkeyLogic Matlab toolbox (31, 32).

Neural Recording Procedures. Single-unit recordings were made from the two M1 monkeys in accordance with a procedure described previously (18). Extracellular potentials were recorded using tungsten electrodes with 0.6 to 1.9 MΩ impedance at 1 kHz (Alpha Omega Engineering; Frederick Haer). Signals were amplified and bandpass-filtered (150 Hz to 8 kHz), and then single-unit activity was isolated using an online template-matching spike discriminator (MAP/OmniPlex system; Plexon). All well-isolated cells were sampled. An oil-driven micromanipulator (MO-971A and MO-972A-D; Narishige) was used to advance an electrode through a stainless-steel guide tube that was held in place by a grid. This grid system allowed recordings every 0.5 mm between penetrations.

Dual-site simultaneous recordings of LFPs were performed in the LH and MPFC using two 16-channel electrodes (U/S-probe; Plexon). The distance between two neighboring channels was 200 μm, and the impedance of each channel was 0.3 to 0.5 MΩ at 1 kHz. LFP signals were amplified, bandpass-filtered (0.2 to 300 Hz), and then digitized at 1 kHz for off-line analysis (OmniPlex system; Plexon).

Identification of Recording Sites.

LH. The recording chamber was tilted 35° laterally in the coronal plane. The physiologically identified LH (see below) spanned ∼6 mm in the rostrocaudal direction with the anterior border roughly corresponding to the level of the anterior commissure (AC), which was overall consistent with prior work (21, 33). During penetrations directed at the anterior LH portion (0 to 2 mm posterior to the AC), the electrode typically passed through the globus pallidus, which was characterized by cells showing large-amplitude spikes and high-frequency discharges (50 to 100 Hz) (34), and then through a thin layer (∼1 mm) of smaller-amplitude cells with lower-frequency discharges, which was considered to correspond to the substantia innominata (35). During penetrations directed at the middle LH portion (3 to 4 mm posterior to the AC), the electrode typically passed through the globus pallidus and the fibers of the internal capsule. During penetrations directed at the posterior LH portion (5 to 6 mm posterior to the AC), the electrode positioned at ventral penetration tracks passed through the subthalamic nucleus and/or the substantia nigra pars reticulata, the firing property of which was consistent with previous studies (34, 36, 37); when the electrode was positioned at more dorsal penetration tracks, it passed through the thalamus, zona incerta, and then the fibers of the H field of Forel. In all portions, LH cells exhibited relatively low spontaneous firing rates of most typically 5 to 10 Hz and relatively broad spike potentials. Moreover, LH activity was frequently modulated by the sight of food, consistent with a previous study (38). The recording site was histologically confirmed (Fig. 1*C*).

MPFC. The recording site in the MPFC included the prefrontal area 9 (39) or 9m (40), as well as its caudally adjacent region known as the presupplementary motor area (pre-SMA). The pre-SMA was physiologically identified on the basis of motor effects evoked by intracortical microstimulation and cellular responses to somatosensory and visual stimuli, as described in detail previously (41, 42). The rostral-most portion of the recording site was 12 mm anterior to the physiological border between the pre-SMA and SMA.

Injection Procedures. After all behavioral and electrophysiological experiments, injection experiments were conducted for the two M1 monkeys. For reversible inactivation of LH cells, a γ-aminobutyric acid agonist, muscimol (Sigma), was used (43). To rule out the possibility that behavioral effects, if any, were caused by increased local pressure due to solution injection, saline vehicle was injected on different days. The amount of solution injected was 1.0 μL for muscimol and 1.0 to 2.0 μL for saline.

For injections of muscimol or saline, we made an injectrode–electrode assembly, that is, a stainless-steel pipe (outer diameter [o.d.], 0.3 mm; inner

diameter [i.d.], 0.17 mm) connected via a Teflon tube (o.d., 0.92 mm; i.d., 0.46 mm) to the needle of a 5-μL Hamilton syringe. A Teflon-coated tungsten wire (A-M Systems) was threaded into the stainless-steel pipe to allow for the continuous monitoring of extracellular single-unit or multiunit activities. Specifically, the injection pipe was lowered to the LH using the oil-driven micromanipulator through the stainless-steel guide tube that was held in place by the grid. After we confirmed that the tip of the injection tube was positioned within the LH, typically at 1 to 2 mm below the dorsolateral border of the LH, injection experiments were started. At each injection site, muscimol or saline was pressure-injected using an injection pump (MD-1001; Bioanalytical Systems, Inc.) at the speed of 0.25 to 0.5 μL/min. Behavioral data collection started 10 min after the end of injections.

For monkey S, seven muscimol injections ($n = 4$ sessions for the right hemisphere, $n = 3$ for the left hemisphere) and four saline injections ($n = 2$ for each hemisphere) were made. For monkey H, four muscimol injections and three saline injections were made in the left hemisphere. Muscimol and saline injections were performed as alternately as possible with at least 3-d intervals separating sessions.

Histology. After all behavioral, electrophysiological, and injection experiments were completed, electrolytic microlesions were made in the LH of monkey S at locations where the electrode entered the LH and task-related cells were recorded. The procedure for histological examinations was described elsewhere (18). Briefly, the monkey was deeply anesthetized and perfused with 0.1 M PBS, followed by 4% formaldehyde and 10% sucrose. Following perfusion, the brain was removed and immersed in a 10% sucrose solution (wt/vol) in 0.1 M phosphate buffer for 7 d and then in a 30% sucrose solution for 21 d. For Nissl staining with cresyl violet, the brain was frozen and cut into 50-μm coronal sections using a sliding microtome equipped with a freezing stage (REM- 710 + Electro Freeze MC-802C; Yamato). Images of each section were taken in bright field under a microscope with a 1× or 4× objective (All-in-one Microscope BZ-9000; Keyence). The LH was then identified from the images.

Statistics. No statistical approach was used to predetermine sample sizes, but our sample sizes were similar to those in previous studies (18, 21, 42). The distribution of data were assumed to be normal, but this was not formally tested. Animals were randomly assigned to M1 or M2 before the initiation of experiments. Visual stimuli were presented pseudorandomly in each trial block. During single-cell recordings in the LH, we mainly sampled cells with firing rates below 30 Hz in accordance with a previous study (21). Data collection and analysis were not performed blind to the experimental conditions. None of the animals was excluded from the study. All statistical procedures (see below) were assessed by two-tailed tests, unless otherwise stated and carried out using commercial software (Matlab 2016a and 2018b; MathWorks).

Data Analysis.

Licking movement. Licking movement that occurred anticipatorily during the stimulus period was quantified and used as a behavioral measure of reward valuation. As described previously (18), licking movements were digitized using a threshold-crossing algorithm. Briefly, signals from the vibration sensor were amplified (50 dB) and filtered (100 to 200 kHz), and their envelopes were sampled at 1 kHz. Each lick was then detected as a discrete event when the envelope signal that had been below a certain threshold value now exceeded another, higher threshold value. The two threshold values were adjusted manually so that the output of licking signals coincided with the mouth movement. The relationship between licking frequency and variable-reward probability was then assessed by correlation testing in each block ($P < 0.05$, Spearman rank correlation test). For analysis here and below, we set two temporal windows: 1) 401 to 800 ms after stimulus onset for the M1-variable block, and 2) 701 to 1,000 ms after stimulus onset for the M2-variable block. The use of different windows between the two trial blocks was determined on the basis of the fact that the licking divergence started earlier in the M1-variable block than in the M2-variable block, as described previously (18).

To assess the impact of muscimol and saline injections on anticipatory licking movement, two statistical tests were performed: Spearman rank correlation test and two-way ANOVA. In the ANOVA, the injection substance (muscimol or saline) and variable-reward probability ($P = 0.25$, 0.50, or 0.75) were used as factors.

Single-cell activity. A total of 379 single LH cells were recorded in the two M1 monkeys. Cellular activity was quantified during the early (151 to 450 ms from stimulus onset) and late (701 to 1,000 ms from stimulus onset) epochs in the stimulus period. In accordance with our previous study (18), the significance of associations between the firing rate and the variable reward probability was separately assessed using linear regression in the M1-variable and M2-variable blocks, and fitted slopes and intercepts were obtained for each cell. On the basis of the significance of the slope coefficient ($P < 0.01$), we then classified individual cells into one of the four types: self, partner, mirror, and value, each of which was further classified as either a positive or negative type. The self-type cells were those exhibiting a significant positive (positive type) or negative (negative type) slope coefficient only in the M1-variable block. The partner-type cells were those exhibiting a significant positive (positive type) or negative (negative type) slope coefficient only in the M2-variable block. The mirror-type cells were those exhibiting a significant positive (positive type) or negative (negative type) slope coefficient in both M1-variable and M2-variable blocks. The positive value-type cells were those exhibiting a significant positive slope coefficient in the M1-variable block and a significant negative slope coefficient in the M2- variable block; conversely, the negative value-type cells were those exhibiting a significant negative slope coefficient in the M1-variable block and a significant positive slope coefficient in the M2-variable block.

For computing the continuous spike-density functions for populations of LH cells, individual spikes were convolved with a Gaussian kernel (SD = 20 ms) for each cell. These values were then averaged separately for each cellular type.

To compare the degree of single-cell activity modulation between the partner–access and partner–no-access conditions in the M2-variable block (Fig. 2*K*), the cellular activity difference for the positive partner-type cells ($n = 21$) was defined as follows: cellular activity difference = [firing rate at P(M2 reward) = 0.75] − [firing rate at P(M2 reward) = 0.25], where P(M2 reward) indicates the M2-reward probability. For the negative partner-type cells ($n = 8$), the following equation was used: cellular activity difference = [firing rate at P(M2 reward) = 0.25] − [firing rate at P(M2 reward) = 0.75]. In both cases, the firing rate in the late epoch was normalized using a z-score normalization procedure applied to each probability condition using the firing rate in the control period (500 to 0 ms before stimulus onset). Outliers were defined as data values exceeding 2.5 SD from the mean, which were removed from further analysis. The cellular activity difference was then compared between the partner–access and partner–no-access conditions ($P < 0.05$; paired t test).

LFPs. The first derivative LFPs from adjacent channels were computed for each 16-channel electrode in the LH and MPFC, generating 15 bipolar LFPs per electrode. This procedure attenuates the effects of electric volume conduction, resulting in more spatially precise evaluation of signal interactions (22).

The latency of LFP modulations from the stimulus onset (Fig. 3*B*) was determined using the procedure described previously (18). First, the bipolar LFPs were averaged across all trials in the two blocks and were processed with a sixth-order low-pass digital Butterworth filter with a 25-Hz cutoff frequency. The data were then converted to z scores relative to the signals in the control period (1,000 to 0 ms before stimulus onset). Finally, the latency was defined as the first bin (1-ms resolution) at which z scores exceeded ±5 SD. Because the detection of early-onset response modulation was the main focus, the latency was included in the analysis when it was earlier than the end of the early epoch (i.e., 450 ms after the stimulus onset).

Field–field coherence. The bipolar LFPs from 1 s before to 3 s after the stimulus onset were concatenated for each recording session into one long time series across all trials in both blocks. The concatenated LFP signals were then convolved with a complex Morlet wavelet function $w(t, f)$:

$$w(t,f) = \sqrt{f}\,\exp\left(-\frac{t^2}{\sigma_t^2}\right)\exp(i2\pi ft),$$

where σ_t is the SD of the Gaussian window at each time bin (t), with the frequency (f) ranging from 1 to 300 Hz (1 to 50 Hz in 1-Hz step, 55 to 75 Hz in 10-Hz step, 90 to 150 Hz in 20-Hz, and 175 to 300 Hz in 25-Hz step). The Morlet wavelet provides high temporal and frequency resolutions for coherence calculation.

The wavelet-transformed concatenated LFPs were divided into the original 4-s LFP segments. Coherence, $C_{xy}(f)$, was then calculated for all LFP pairs within the LH and between LH and MPFC using the following equation:

$$C_{xy}(f) = \left|\frac{G_{xy}(f)G_{xy}^{*}(f)}{G_{xx}(f)G_{yy}(f)}\right|,$$

where $G_{xy}(f)$ is the cross-spectrum and $G_{xx}(f)$ and $G_{yy}(f)$ are the autospectram, with * denoting the complex conjugate. Coherence $C_{xy}(f)$ ranges between 0 and 1, with 1 being complete coherence and 0 being complete independence. That is, the coherence at frequency (f) approaches 1 when there is a constant phase and amplitude relationship at frequency (f) between two LFP signals over

trials (44). The above procedures minimized trial-specific variance and edge artifact of low-frequency wavelets. They also ensured that the duration of LFP signals was long enough for low-frequency coherence analyses.

For statistical and illustrative purposes, the coherence data from 0.5 s before to 1.0 s after the stimulus onset were extracted and averaged separately for each block (M1-variable and M2-variable). The coherence value in individual sessions was normalized using a *z*-transformation. For this purpose, the mean and SD in the baseline period (−0.5 to 0 s from the stimulus onset) was calculated using the two blocks combined together. The median value from all sessions was plotted to visualize time-dependent changes of coherence (Fig. 3*C*).

Granger causality. A Granger causality analysis (45) was applied to simultaneously recorded LFPs to determine the direction of information flow between LH and MPFC. This analysis was implemented by using a multivariate linear vector autoregressive (MVAR) model provided by the Multivariate Granger Causality toolbox (46) in the frequency domain between 1 and 300 Hz with a 1.67-Hz resolution, as described in detail elsewhere (18). Specifically, the bipolar LFPs obtained from adjacent channels were used to eliminate spurious causalities. For these data, the best model order was estimated using the Akaike information criteria up to 50 ms. Next, the MVAR model parameters for the selected model order were estimated using ordinary least-squares regression. LFP time series data with problems of collinearity, nonstationarity, or heteroscedasticity were excluded. For LFP signals without these problems, the autocovariance sequence from the MVAR parameters was calculated. Finally, the time-domain pairwise conditional Granger causality was estimated by *F* testing with false discovery rate at each frequency ($Q < 0.05$).

The proportion of the bipolar LFP pairs showing significant Granger causality was measured in the LH-to-MPFC direction and the MPFC-to-LH direction for each task epoch (i.e., early and late). The proportion of significant causality pairs was then compared between the two directions for each frequency band (δ, 1 to 3 Hz; θ, 4 to 7 Hz; α, 8 to 12 Hz; low β, 13 to 20 Hz; high β, 21 to 30 Hz; low γ, 31 to 49 Hz; high γ, 50 to 300 Hz; Welch's *t* test, $P < 0.05$; Fig. 3 *D*, *Bottom*).

Data Availability. All data discussed in the paper are available in the main text and *SI Appendix*.

ACKNOWLEDGMENTS. We thank M. Yoshida, S. Tomatsu, I. Yokoi, N. Goda, A. Uematsu, and Y. Yamazaki for helpful discussions; Y. Ueda for preparing injectrode–electrode assemblies; and M. Togawa, Y. Yamanishi, T. Jochi, K. Takada, and A. Shibata for technical assistance. Japanese monkeys were provided by the National Bio-Resource Project "Japanese Macaques" of Japan Agency for Medical Research and Development (AMED). This work was supported in part by Grants-in-Aid for Japan Society for the Promotion of Science (KAKENHI Grants 15K04200 and 18K03194) (A.N.) and by AMED under Grant JP19dm0107145 (M.I.).

1. A. B. Butler, W. Hodos, *Comparative Vertebrate Neuroanatomy: Evolution and Adaptation* (Wiley, ed. 2, 2005).
2. S. V. Mahler, D. E. Moorman, R. J. Smith, M. H. James, G. Aston-Jones, Motivational activation: A unifying hypothesis of orexin/hypocretin function. *Nat. Neurosci.* **17**, 1298–1303 (2014).
3. G. D. Petrovich, Lateral hypothalamus as a motivation-cognition interface in the control of feeding behavior. *Front. Syst. Neurosci.* **12**, 14 (2018).
4. P. Bonnavion, L. E. Mickelsen, A. Fujita, L. de Lecea, A. C. Jackson, Hubs and spokes of the lateral hypothalamus: Cell types, circuits and behaviour. *J. Physiol.* **594**, 6443–6462 (2016).
5. R. M. Chemelli *et al*., Narcolepsy in orexin knockout mice: Molecular genetics of sleep regulation. *Cell* **98**, 437–451 (1999).
6. A. R. Adamantidis, F. Zhang, A. M. Aravanis, K. Deisseroth, L. de Lecea, Neural substrates of awakening probed with optogenetic control of hypocretin neurons. *Nature* **450**, 420–424 (2007).
7. G. C. Harris, M. Wimmer, G. Aston-Jones, A role for lateral hypothalamic orexin neurons in reward seeking. *Nature* **437**, 556–559 (2005).
8. P. Bonnavion, A. C. Jackson, M. E. Carter, L. de Lecea, Antagonistic interplay between hypocretin and leptin in the lateral hypothalamus regulates stress responses. *Nat. Commun.* **6**, 6266 (2015).
9. Á. Flores, R. Saravia, R. Maldonado, F. Berrendero, Orexins and fear: Implications for the treatment of anxiety disorders. *Trends Neurosci.* **38**, 550–559 (2015).
10. S. Cole, M. P. Hobin, G. D. Petrovich, Appetitive associative learning recruits a distinct network with cortical, striatal, and hypothalamic regions. *Neuroscience* **286**, 187–202 (2015).
11. M. J. Sharpe *et al*., Lateral hypothalamic GABAergic neurons encode reward predictions that are relayed to the ventral tegmental area to regulate learning. *Curr. Biol.* **27**, 2089–2100.e5 (2017).
12. D. Ongür, X. An, J. L. Price, Prefrontal cortical projections to the hypothalamus in macaque monkeys. *J. Comp. Neurol.* **401**, 480–505 (1998).
13. J. Jin *et al*., Orexin neurons in the lateral hypothalamus project to the medial prefrontal cortex with a rostro-caudal gradient. *Neurosci. Lett.* **621**, 9–14 (2016).
14. C. J. Reppucci, G. D. Petrovich, Organization of connections between the amygdala, medial prefrontal cortex, and lateral hypothalamus: A single and double retrograde tracing study in rats. *Brain Struct. Funct.* **221**, 2937–2962 (2016).
15. E. H. Nieh *et al*., Inhibitory input from the lateral hypothalamus to the ventral tegmental area disinhibits dopamine neurons and promotes behavioral activation. *Neuron* **90**, 1286–1298 (2016).
16. M. P. Noonan *et al*., A neural circuit covarying with social hierarchy in macaques. *PLoS Biol.* **12**, e1001940 (2014).
17. F. Kurth *et al*., Diminished gray matter within the hypothalamus in autism disorder: A potential link to hormonal effects? *Biol. Psychiatry* **70**, 278–282 (2011).
18. A. Noritake, T. Ninomiya, M. Isoda, Social reward monitoring and valuation in the macaque brain. *Nat. Neurosci.* **21**, 1452–1462 (2018).
19. L. Festinger, A theory of social comparison processes. *Hum. Relat.* **7**, 117–140 (1954).
20. D. M. Amodio, C. D. Frith, Meeting of minds: The medial frontal cortex and social cognition. *Nat. Rev. Neurosci.* **7**, 268–277 (2006).
21. A. Noritake, K. Nakamura, Encoding prediction signals during appetitive and aversive Pavlovian conditioning in the primate lateral hypothalamus. *J. Neurophysiol.* **121**, 396–417 (2019).
22. T. Ninomiya, K. Dougherty, D. C. Godlove, J. D. Schall, A. Maier, Microcircuitry of agranular frontal cortex: Contrasting laminar connectivity between occipital and frontal areas. *J. Neurophysiol.* **113**, 3242–3255 (2015).
23. G. Michalareas *et al*., Alpha-beta and gamma rhythms subserve feedback and feedforward influences among human visual cortical areas. *Neuron* **89**, 384–397 (2016).
24. M. Trusel *et al*., Punishment-predictive cues guide avoidance through potentiation of hypothalamus-to-habenula synapses. *Neuron* **102**, 120–127.e4 (2019).
25. F. Grabenhorst, R. Baez-Mendoza, W. Genest, G. Deco, W. Schultz, Primate amygdala neurons simulate decision processes of social partners. *Cell* **177**, 986–998.e15 (2019).
26. S. W. Chang *et al*., Neural mechanisms of social decision-making in the primate amygdala. *Proc. Natl. Acad. Sci. U.S.A.* **112**, 16012–16017 (2015).
27. G. Mancini, P. F. Ferrari, E. Palagi, Rapid facial mimicry in geladas. *Sci. Rep.* **3**, 1527 (2013).
28. N. L. Rempel-Clower, H. Barbas, Topographic organization of connections between the hypothalamus and prefrontal cortex in the rhesus monkey. *J. Comp. Neurol.* **398**, 393–419 (1998).
29. S. Manita *et al*., A top-down cortical circuit for accurate sensory perception. *Neuron* **86**, 1304–1316 (2015).
30. National Research Council, *Guide for the Care and Use of Laboratory Animals* (National Academies Press, Washington, DC, ed. 8, 2011).
31. W. F. Asaad, E. N. Eskandar, Achieving behavioral control with millisecond resolution in a high-level programming environment. *J. Neurosci. Methods* **173**, 235–240 (2008).
32. W. F. Asaad, E. N. Eskandar, A flexible software tool for temporally-precise behavioral control in Matlab. *J. Neurosci. Methods* **174**, 245–258 (2008).
33. T. Kusama, M. Mabuchi, *Stereotaxic Atlas of the Brain of Macaca fuscata* (University of Tokyo Press, Tokyo, Japan, 1970).
34. M. R. DeLong, M. D. Crutcher, A. P. Georgopoulos, Primate globus pallidus and subthalamic nucleus: Functional organization. *J. Neurophysiol.* **53**, 530–543 (1985).
35. F. A. Wilson, E. T. Rolls, Neuronal responses related to the novelty and familarity of visual stimuli in the substantia innominata, diagonal band of Broca and periventricular region of the primate basal forebrain. *Exp. Brain Res.* **80**, 104–120 (1990).
36. O. Hikosaka, R. H. Wurtz, Visual and oculomotor functions of monkey substantia nigra pars reticulata. I. Relation of visual and auditory responses to saccades. *J. Neurophysiol.* **49**, 1230–1253 (1983).
37. M. Isoda, O. Hikosaka, Role for subthalamic nucleus neurons in switching from automatic to controlled eye movement. *J. Neurosci.* **28**, 7209–7218 (2008).
38. E. T. Rolls, M. J. Burton, F. Mora, Hypothalamic neuronal responses associated with the sight of food. *Brain Res.* **111**, 53–66 (1976).
39. H. Barbas, D. N. Pandya, Architecture and intrinsic connections of the prefrontal cortex in the rhesus monkey. *J. Comp. Neurol.* **286**, 353–375 (1989).
40. S. Miyachi *et al*., Organization of multisynaptic inputs from prefrontal cortex to primary motor cortex as revealed by retrograde transneuronal transport of rabies virus. *J. Neurosci.* **25**, 2547–2556 (2005).
41. M. Isoda, O. Hikosaka, Switching from automatic to controlled action by monkey medial frontal cortex. *Nat. Neurosci.* **10**, 240–248 (2007).
42. K. Yoshida, N. Saito, A. Iriki, M. Isoda, Social error monitoring in macaque frontal cortex. *Nat. Neurosci.* **15**, 1307–1312 (2012).
43. O. Hikosaka, R. H. Wurtz, Modification of saccadic eye movements by GABA-related substances. I. Effect of muscimol and bicuculline in monkey superior colliculus. *J. Neurophysiol.* **53**, 266–291 (1985).
44. M. X. Cohen, *Analyzing Neural Time Series Data: Theory and Practice* (The MIT Press, Cambridge, MA, 2014).
45. C. W. J. Granger, Investigating causal relations by econometric models and cross-spectral methods. *Econometrica* **37**, 424–438 (1969).
46. L. Barnett, A. K. Seth, The MVGC multivariate Granger causality toolbox: A new approach to Granger-causal inference. *J. Neurosci. Methods* **223**, 50–68 (2014).